Sensors and Materials, Vol. 38, No. 5 (2026) 2491–2506
MYU Tokyo

S & M 4449

Performance Improvement of Sensor-based Robotic Arm Control Strategy in Noisy Environments

Di Zhang, Xiaoyu Bian, Shuhua Miao, Siyuan Chen, Rui Ma, Zixuan Yuan, and Lingling Li*

Hebei University of Technology, Tianjin 300401, China

(Received February 10, 2026; accepted April 13, 2026)

Keywords: robotic manipulator, sensor noise, multisensor fusion, extended Kalman filter, trajectory tracking

Sensor noise significantly degrades the trajectory tracking accuracy of robotic manipulators. In this paper, we propose a closed-loop control strategy based on multisensor fusion and an extended Kalman filter (EKF) to enhance performance under noisy sensing conditions. A six-degree-of-freedom Puma 560 manipulator is modeled, including its kinematics, dynamics, and stochastic measurement models for encoders and an inertial measurement unit. The EKF fuses multisensor data to provide real-time estimates of joint positions and velocities, which are integrated into a computed torque controller. Comparative simulations in Matrix Laboratory/Simulink demonstrate that, compared with conventional feedback using direct noisy measurements, the proposed approach reduces end-effector position error, suppresses velocity estimation fluctuations, and achieves smoother trajectory tracking. We validate the effectiveness of EKF-based sensor fusion for improving the robustness of robotic manipulators in noise-affected environments. All results are obtained from simulations and have not been validated on physical hardware; sensor non-Gaussian noise, sudden faults, and joint flexibility are not considered. Future work will focus on hardware-in-the-loop validation, adaptive robust filtering, and deep-learning-assisted noise modeling to address these limitations.

1. Introduction

The high-precision control of robotic manipulators is crucial in industrial manufacturing and precision assembly. Such control relies on sensors, such as encoders and inertial measurement units (IMUs), to provide joint position and velocity information. As demands for precision grow, control performance has become increasingly dependent on the quality of these sensor measurements.

Sensor noise remains a major practical challenge, as disturbances from Gaussian noise, bias drift, and quantization errors degrade trajectory tracking accuracy, especially under dynamic conditions. Conventional control strategies using raw measurements directly show limited robustness to such disturbances. While various filtering and observer-based methods exist, they

*Corresponding author: e-mail: lilingling@hebut.edu.cn
https://doi.org/10.18494/SAM6279

ISSN 0914-4935
https://myukk.org/

often involve trade-offs between noise suppression and dynamic response, and may not fully exploit system dynamics.

Multisensor fusion has therefore emerged as an effective approach to improve state estimation accuracy in noisy environments. By combining complementary sensor information, fusion techniques enhance robustness against individual sensor limitations. The extended Kalman filter (EKF) is widely used for nonlinear systems owing to its ability to incorporate system models and stochastic noise characteristics. Although EKF has been successfully applied in areas such as mobile robot navigation, its integration with model-based control for robotic manipulators under sensor noise conditions warrants further investigation.[1,2] Different from existing works that primarily apply EKF for mobile robot localization or single-joint control, in this paper, we deeply couple EKF with computed torque control in a full closed-loop framework for a six-degree-of-freedom serial manipulator. The proposed approach not only quantifies the improvement in trajectory tracking accuracy but also provides a performance benchmark for sensor selection and noise specification in robotic systems.

Beyond control performance improvement, a method for guiding the design and selection of sensors using the proposed fusion framework was demonstrated in this study, contributing to the field of sensors and sensing. Specifically, the EKF-based fusion reveals the required noise characteristics and bandwidth for encoders and IMUs to achieve a given control accuracy. The simulation framework can serve as a tool for evaluating different sensor configurations before hardware implementation, thereby reducing development cost and time.

In this study, we propose a closed-loop control framework for robotic manipulators based on multisensor fusion and EKF-based state estimation. A six-degree-of-freedom Puma 560 manipulator is modeled, including kinematic, dynamic, and stochastic sensor models for encoders and an IMU. The EKF provides real-time estimates of joint states, which are fed into a computed torque controller. Comparative simulations in MATLAB/Simulink demonstrate that the proposed method improves trajectory tracking performance under noisy conditions compared with conventional feedback control using raw measurements.

2. Robotic Arm System and Sensor Modeling

2.1 Kinematic and dynamic modeling of six-degree-of-freedom robotic arm

The robotic manipulator investigated in this study is a six-degree-of-freedom Puma 560 arm, as shown in Fig. 1. All six joints are revolute joints. Joints 1–3 mainly determine the position of the end effector, whereas joints 4–6 control its orientation. The Denavit–Hartenberg (D–H) convention is employed to establish the coordinate frames. The D–H parameters of the Puma 560 manipulator used in this study are summarized in Table 1.

The homogeneous transformation matrix between two adjacent frames is expressed as

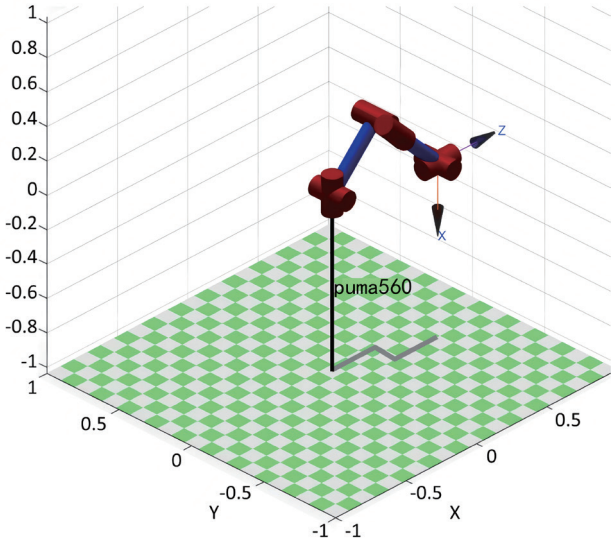

Fig. 1. (Color online) Structure of Puma 560 six-axis robotic arm.

Table 1
Denavit–Hartenberg parameters of six-degree-of-freedom robotic arm.

Link i	Joint angle (rad)	Link length (m)	Link twist (rad)	Joint offset (m)	Offset
1	—	0	0	0	0
2	—	0.4318	0	0	0
3	—	0.0203	0	0.15005	0
4	—	0	0	0.4318	0
5	—	0	0	0	0
6	—	0	0	0	0

$$ {}^{i}_{i-1}T = \begin{bmatrix} \cos\theta_i & -\sin\theta_i \cos\alpha_{i-1} & \sin\theta_i \sin\partial_{i-1} & a_{i-1}\cos\theta_i \\ \sin\theta_i & \cos\theta_i \cos\partial_{i-1} & -\cos\theta_i \sin\partial_{i-1} & a_{i-1}\sin\alpha_{i-1} \\ 0 & \sin\partial_{i-1} & \cos\partial_{i-1} & d_i \\ 0 & 0 & 0 & 1 \end{bmatrix}. \tag{1} $$

The forward kinematics of the manipulator is obtained by cascading the homogeneous transformation matrices from the base to the end effector.

The dynamic model of the robotic arm is derived using the Lagrangian formulation under assumptions of rigid links and joint backlash is neglected.

$$ M(\theta)\ddot{\theta} + C\left(\theta, \dot{\theta}\right) + G(\theta) = \tau \tag{2} $$

Here, $M(\theta)$ is the symmetric positive-definite mass matrix, $C(\theta, \dot{\theta})$ represents the Coriolis and centrifugal terms, $G(\theta)$ is the gravity vector, and τ denotes the generalized joint torque.[3] This

model is used in the EKF prediction step to propagate state estimates between sensor measurements.

2.2 Closed-loop control framework and state feedback requirements

In open-loop control, the joint torque τ is calculated directly from the inverse kinematics model without real-time feedback, which lacks error correction capability. Therefore, state feedback is essential to achieve high-precision control under noisy conditions. The system state vector is defined as

$$X = \left[\theta_1, \theta_2, \theta_3, \theta_4, \theta_5, \theta_6, \dot{\theta}_1, \dot{\theta}_2, \ldots, \dot{\theta}_6\right]^T = \left[\theta^T, \dot{\theta}^T\right]^T, \tag{3}$$

which includes joint positions and joint velocities. These state variables cannot be directly observed. A sensor-based closed-loop control framework is therefore adopted, as illustrated in Fig. 2, in which real-time state information is used to dynamically adjust the control input.

2.3 Sensor measurement models

To meet the requirements of state feedback, two types of sensor are employed: joint encoders and an IMU. The encoder measurement is modeled as

$$Z_{enc}(k) = \theta(k) + V_{enc}(k), \tag{4}$$

where $V_{enc}(k)$ represents zero-mean Gaussian measurement noise.

An IMU mounted on the end effector provides three-dimensional motion information. The gyroscope and accelerometer measurement models are given by

$$Z_{gyro}(k) = R_T^B(k) \cdot \omega^B(k) + b_g(k) + V_g(k), \tag{5}$$

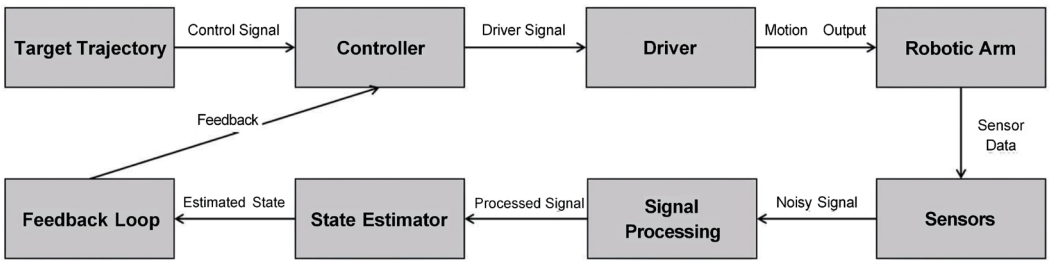

Fig. 2. Closed-loop control framework used in this study.

$$Z_{acc}(k) = R_T^B(k) \cdot \left(a^B(k) - g^B\right) + b_a(k) + V_a(k), \tag{6}$$

where $\omega^B(k)$ and $a^B(k)$ are the true angular velocity and linear acceleration, respectively, $b_g(k)$ and $b_a(k)$ are sensor biases, and $V_g(k)$ and $V_a(k)$ are Gaussian noise vectors.

The combined measurement model is expressed as

$$Z(k) = h\left(X(k)\right) + V(k), \tag{7}$$

where $h(\cdot)$ is the nonlinear observation function and $V(k)$ is the measurement noise vector.

2.4 Sensor noise, bias, and outlier modeling

In practical applications, sensor measurements are affected by noise, bias drift, and occasional outliers. To account for these effects, the measurement models are extended as follows.

Encoder noise is modeled as additive Gaussian white noise with the covariance matrix R_{enc}. For the IMU, the gyroscope noise $V_g \sim N(0, Q_g)$ and the accelerometer noise $V_a \sim N(0, Q_a)$ are considered. The sensor biases b_g and b_a are modeled as first-order Gauss−Markov processes. To enhance robustness against abnormal measurements, adaptive covariance adjustment or robust kernel functions can be introduced.[4]

The complete stochastic measurement model is given by

$$Z(k) = h\left(X(k)\right) + b(k) + S(k)V(k), \tag{8}$$

where $b(k)$ represents the bias vector and $S(k)$ is a noise scaling matrix.

3. Sensor Signal Processing Algorithm

3.1 Effect of sensor noise on control signals

In the closed-loop control of robotic manipulators, sensor measurements are directly used to construct joint position and velocity feedback signals. When measurement noise is present, estimation errors propagate through the feedback loop and affect the control input, leading to degraded trajectory smoothness and increased tracking errors.

In particular, joint velocity information is highly sensitive to measurement noise. When velocities are obtained from discrete sensor measurements, noise components may be amplified and injected into the control torque through derivative feedback and dynamic compensation terms. As a result, the direct utilization of raw sensor signals is insufficient for achieving high-precision control under noisy sensing conditions, motivating the use of model-based state estimation methods.

3.2 Necessity of model-based signal filtering

Conventional filtering techniques, such as moving-average or low-pass filtering, can suppress high-frequency noise but often introduce phase delay and reduce dynamic responsiveness. Moreover, these techniques do not explicitly exploit the system dynamics and therefore have limited effectiveness in nonlinear robotic systems.

To overcome these limitations, model-based filtering techniques that combine sensor measurements with system dynamics are required. Kalman filtering provides an optimal recursive estimation framework under Gaussian noise assumptions and is therefore well suited for processing noisy sensor data in robotic control systems.[5,6]

3.3 Extended Kalman filter for nonlinear robotic systems

The kinematics and dynamics of robotic manipulators generally exhibit strong nonlinear characteristics. The discrete-time nonlinear state-space model of a robotic system can be expressed in a generalized form as

$$X(k+1) = f\left(X(k)\right) + G(k)W(k), \tag{9}$$

where $f(\cdot)$ denotes the nonlinear state transition function, $W(k)$ represents the process noise, and $G(k)$ is the process noise input matrix (noise gain matrix). It is usually assumed that $W(k) \sim N(0, Q(k))$ and the measurement model follows the formulation given in Sect. 2.3.

Since the standard Kalman filter requires the system model to be linear, the above nonlinear model must be locally linearized. The core idea of the EKF is to perform a first-order Taylor expansion of the nonlinear functions around the current state estimate. The Jacobian matrices

$$\Phi\left(k+1\,|k\right) = \frac{\partial f}{\partial X}, H\left(k+1\right) = \frac{\partial h}{\partial X} \tag{10}$$

are obtained through this linearization process, transforming the original nonlinear system into a time-varying linear system in the neighborhood of the current estimate.[7–9]

The recursive procedure of the EKF then follows the standard Kalman filtering framework, consisting of state prediction, covariance prediction, Kalman gain calculation, state update, and covariance update.[10,11]

4. Control Strategy Based on Sensor Feedback

4.1 Robotic manipulator position control model

To achieve high-precision trajectory tracking, a closed-loop control law is designed on the basis of the dynamic model established in Sect. 2. Considering the complete dynamic equation of the PUMA 560 manipulator [Eq. (2)], the joint-space tracking errors are defined as

$$e = \theta_d - \theta, \dot{e} = \dot{\theta}_d - \dot{\theta}, \tag{11}$$

where $\theta_d(t)$, $\dot{\theta}_d(t)$, and $\ddot{\theta}_d(t)$ denote the desired joint position, velocity, and acceleration trajectories, respectively. Let K_P and K_D be positive definite diagonal proportional and derivative gain matrices, respectively. The ideal control law based on the computed torque method is designed as

$$\tau = M(\theta)\left[\ddot{\theta}_d + K_D\dot{e} + K_P e\right] + C\left(\theta,\dot{\theta}\right) + G(\theta). \tag{12}$$

Under the assumption of a perfectly accurate model, substituting Eq. (2) into Eq. (12) yields the closed-loop error dynamics $\ddot{e} + K_D\dot{e} + K_P e = 0$. By appropriately selecting the positive definite gain matrices K_P and K_D, the tracking error can be guaranteed to converge asymptotically to zero.

However, two major challenges arise in practical systems. First, the controller relies on the approximate models $\hat{M}$, $\hat{C}$, and $\hat{G}$ based on nominal parameters. Second, the true joint states θ and $\dot{\theta}$ cannot be directly obtained and must be estimated from sensor measurements.[12,13]

4.2 Control method based on sensor measurements

In this paper, we propose a conventional control implementation that directly utilizes raw sensor measurements. In practical applications, the control law in Eq. (12) must be reformulated using available measurement information. Encoder measurements $Z_{enc}(k)$ [Eq. (4)] are used as the joint position estimate $\theta_m(k)$, and the joint velocity is obtained via backward numerical differentiation:

$$\dot{\theta}_m(k) = \frac{\theta_m(k) - \theta_m(k-1)}{\Delta T}, \tag{13}$$

where ΔT is the control sampling period. On the basis of these measured quantities, the practical control law can be expressed as

$$\tau_{meas} = \hat{M}(\theta_m)\left[\ddot{\theta}_m + K_D\left(\dot{\theta}_d - \dot{\theta}_m\right) + K_P\left(\theta_d - \theta_m\right)\right] + \hat{C}\left(\theta_m,\dot{\theta}_m\right) + G(\theta_m). \tag{14}$$

This control structure is widely used in industrial applications; however, its performance is severely constrained by two sources of noise. The position measurement noise V_{enc} directly enters the position feedback channel, whereas the velocity estimate $\dot{\theta}_m$ obtained through numerical differentiation contains significantly amplified high-frequency noise components.

The numerical differentiation process essentially acts as a high-pass operation. Under a typical millisecond-level control period (ΔT = 0.001 s), high-frequency noise may be amplified

by several orders of magnitude and injected into the control torque through the derivative gain K_D, potentially causing high-frequency actuator oscillations.

To ensure stability, conservative design choices are often required, such as limiting the derivative gain K_D, introducing additional low-pass filters in the feedback loop. Although these measures improve stability, they do so at the cost of reduced dynamic response and tracking accuracy. Furthermore, the use of noisy velocity estimates in computing the Coriolis and centrifugal compensation term introduces additional feedforward errors, further degrading end-effector positioning accuracy.[14]

4.3 Control improvement based on EKF state estimation

To fundamentally address the performance limitations of the conventional approach, an enhanced control strategy based on the EKF algorithm presented in Sect. 3 is proposed. The core idea is to replace raw sensor measurements with optimal state estimates as feedback signals.

According to the EKF formulation in Sect. 3.3, the algorithm provides the optimal state estimate at each time step k as

$$\hat{X}(k \mid k) = \begin{bmatrix} \hat{\theta}(k \mid k) \\ \hat{\dot{\theta}}(k \mid k) \end{bmatrix}, \tag{15}$$

where $\hat{\theta}(k \mid k) \in \mathbb{R}^6$ denotes the optimal joint position estimate and $\hat{\dot{\theta}}(k \mid k) \in \mathbb{R}^6$ denotes the optimal joint velocity estimate. These estimates are obtained by fusing encoder measurements $Z_{enc}(k)$ [Eq. (4)] with IMU measurements $Z_{gyro}(k)$, $Z_{acc}(k)$ [Eqs. (5) and (6)], using the robotic manipulator dynamic model [Eq. (2)].

The key feature of the proposed strategy is the upgrade of the feedback source. The optimal state estimates provided by the EKF completely replace the raw measured quantities θ_m and $\dot{\theta}_m$. Accordingly, the control law is reformulated as

$$\tau_{EKF} = \hat{M}\left(\hat{\theta}\right)\left[\ddot{\theta}_d + K_D\left(\dot{\theta}_d - \hat{\dot{\theta}}\right) + K_P\left(\theta_d - \hat{\theta}\right)\right] + C\left(\theta, \dot{\theta}\right) + G\left(\hat{\theta}\right). \tag{16}$$

By integrating multisensor fusion with model-based prediction, the EKF significantly improves the quality of state estimation. Encoders provide reliable absolute position references, while IMUs offer high-frequency differential information. The EKF optimally fuses the complementary characteristics of both sensors. More importantly, the prediction step of the EKF is driven by the system dynamics, forming an adaptive, model-based filtering mechanism. Compared with fixed numerical differentiation, this approach more effectively suppresses noise without introducing additional phase lag.

The effectiveness of dynamic feedforward compensation strongly depends on the accuracy of velocity information. In conventional methods, errors in numerically differentiated velocities propagate into the Coriolis and centrifugal compensation term $\hat{C}(\theta_m, \dot{\theta}_m)$. In contrast, the smooth

velocity estimates provided by the EKF significantly improve the accuracy of nonlinear compensation, reducing the burden on the feedback loop.

Under time-varying noise or impulsive disturbances, the EKF framework offers additional robustness mechanisms through the adaptive adjustment of noise covariance or the incorporation of robust kernel functions, as discussed in Sect. 2.4. This ensures that state estimation remains reliable even under adverse sensing conditions, directly enhancing the control system's tolerance to temporary sensor degradation or sudden disturbances.[15–17]

5. Simulation Experiments and Results

5.1 Simulation platform and experimental setup

To verify the effectiveness of the proposed robotic manipulator control strategy based on multisensor fusion and the EKF under noisy conditions, a six-degree-of-freedom Puma 560 robotic arm simulation system was developed in the MATLAB environment. The kinematic and dynamic models of the manipulator were constructed on the basis of the mathematical formulations established in Sect. 2, and the controller structure adopted the computed torque control method designed in Sect. 4.

In the simulation experiments, the end effector was commanded to follow a circular trajectory in the operational space. The trajectory was mainly distributed in the XY plane, while the Z-direction position remained approximately constant, representing a typical planar precision manipulation task. The corresponding joint-space reference trajectories were obtained through inverse kinematics and used as the desired inputs of the control system.

To simulate measurement uncertainties encountered in real industrial environments, Gaussian white noise and bias drift were introduced into the encoder and IMU sensor outputs. Specifically, encoder noise was set with a standard deviation of 0.001 rad, gyroscope noise with 0.005 rad/s, and accelerometer noise with 0.01 m/s², and bias drifts were modeled as first-order Gauss–Markov processes with a correlation time constant of 100 s. Three operating conditions were considered for comparative analysis:

(1) baseline control under ideal noise-free conditions,
(2) conventional feedback control using direct noisy sensor measurements, and
(3) sensor fusion control based on EKF state estimation.

5.2 Baseline performance and noise-induced degradation

Under ideal noise-free conditions, the joint angle responses of the six-degree-of-freedom Puma 560 robotic arm are as shown in Fig. 3(a). It can be observed that all joint angles exhibit smooth and continuous periodic variations over time, without notable oscillations or numerical instability. This indicates that, under nominal model conditions, the designed control system is capable of achieving stable joint-space trajectory tracking. These results serve as a baseline reference for subsequent performance analysis under noisy sensing conditions.

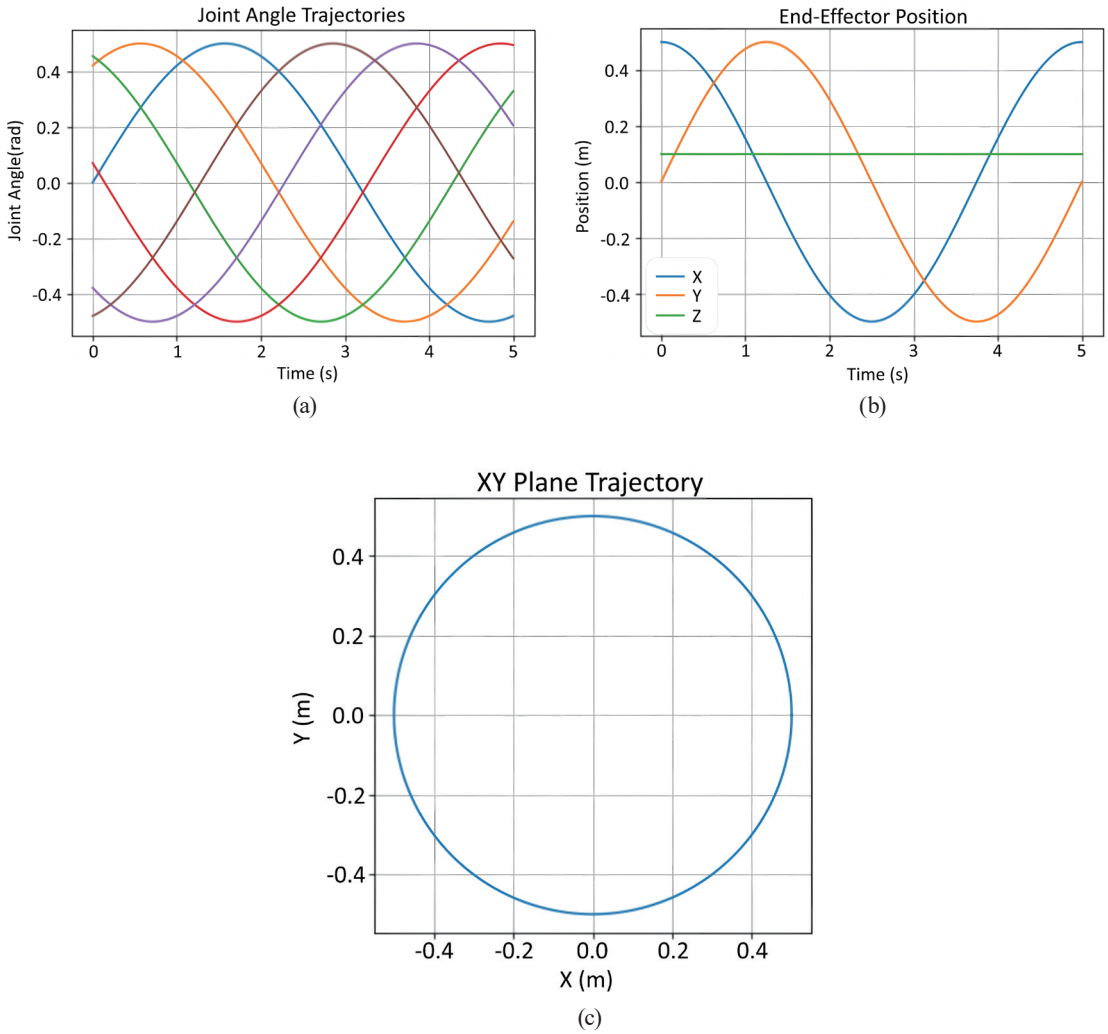

Fig. 3. (Color online) Baseline performance under ideal noise-free conditions: (a) joint angles, (b) end-effector positions, and (c) *XY* trajectory.

The position responses of the end effector in task space are illustrated in Fig. 3(b). Periodic variations can be observed along the *X*- and *Y*-directions, while the displacement along the *Z*-direction remains nearly constant. This confirms that the end-effector motion is mainly confined to the *XY* plane, consistent with the prescribed planar circular trajectory.

The corresponding trajectory of the end effector in the *XY* plane is as shown in Fig. 3(c). The trajectory forms a regular circular shape with good continuity, indicating that under noise-free conditions, the trajectory planning and inverse kinematics solution can accurately reproduce the desired geometric path.

After introducing noise into the encoder and IMU measurement signals, the time evolution of the end-effector position error is as shown in Fig. 4(a). The error exhibits random fluctuations throughout the simulation, reflecting the persistent effect of sensor noise on end-effector position measurements.

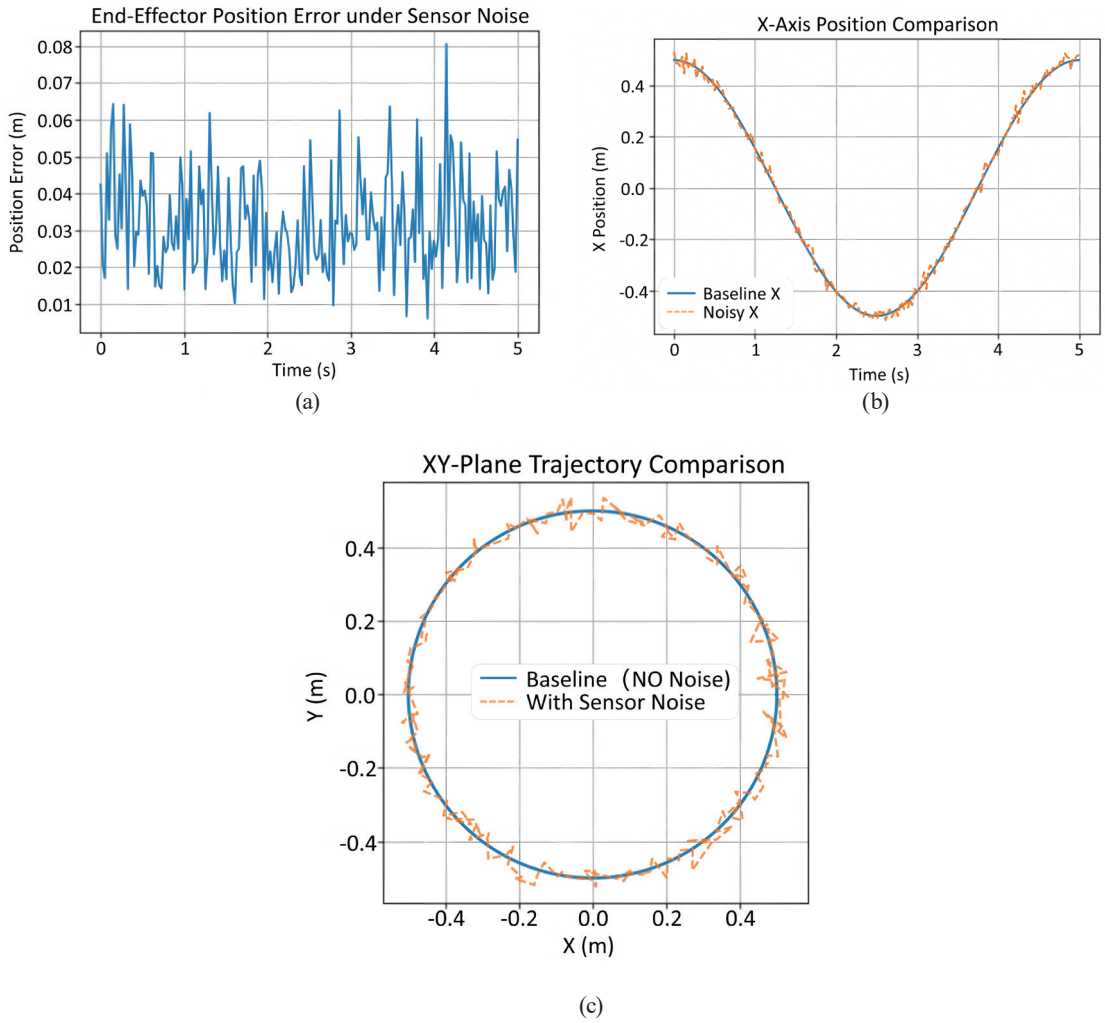

Fig. 4. (Color online) Performance degradation under sensor noise: (a) end-effector position error, (b) *X*-axis position comparison, and (c) baseline end-effector trajectory in *XY* plane.

Taking the *X*-direction displacement as an example, Fig. 4(b) shows a comparison of the responses under noise-free and noisy conditions. Compared with the baseline trajectory, the noisy response shows pronounced high-frequency oscillations, indicating that measurement noise propagates through the feedback loop and is amplified in the output response.

From a task-space geometric perspective, the end-effector trajectory in the *XY* plane under noisy conditions is as shown in Fig. 4(c). Compared with the ideal circular trajectory, the actual trajectory deviates irregularly around the desired path, with reduced smoothness and geometric consistency. These results demonstrate that sensor noise not only affects instantaneous position responses but also degrades the overall trajectory quality in task space.

When noisy measurements are directly used for feedback control, the end-effector position error exhibits significant random fluctuations over time, with the main distribution range approximately between 0.02 and 0.05 m, accompanied by occasional peaks. To avoid the effects

of initial and terminal transients on statistical results, the steady-state interval from $t = 0.3$ to 4.7 s was selected for quantitative evaluation.

Statistical analysis shows that under this operating condition, as shown in Table 2, the mean end-effector position error is 0.0309 m, the root mean square error (*RMSE*) is 0.0325 m, and the maximum error reaches 0.0670 m. These results indicate that sensor noise significantly increases both the magnitude and variability of tracking errors.

Using the *X*-direction response as a representative case, we observed notable oscillations in the noisy feedback curve relative to the baseline trajectory. The statistical analysis of the *X*-direction deviation over the steady-state interval, as also summarized in Table 2, yields a mean absolute error (*MAE*) of 0.0118 m, an *RMSE* of 0.0141 m, and a maximum deviation of 0.0505 m. This confirms that measurement noise not only introduces random disturbances but also causes large instantaneous deviations at certain time instants.

5.3 EKF-based fusion control performance improvement

After introducing EKF-based state estimation, the three-dimensional task-space trajectory of the end effector is as shown in Fig. 5(a). Compared with the results obtained using direct noisy measurement feedback in Sect. 5.2, the trajectory under EKF-based control is significantly smoother. The end-effector motion maintains good continuity throughout the simulation, without notable high-frequency oscillations caused by sensor noise. This indicates that the EKF effectively fuses encoder and IMU information and suppresses measurement noise under the constraints of the system model.

To further analyze the effect of the EKF on state estimation quality, Fig. 5(b) presents a comparison of end-effector responses along the *X*-direction, including the baseline trajectory, the noisy measurement feedback result, and the EKF-based estimation result. The EKF-based response closely follows the baseline trajectory in overall trend, while significantly attenuating the high-frequency fluctuations observed in the noisy response. Compared with direct measurement-based feedback, the EKF achieves effective noise suppression without introducing notable phase delay, demonstrating superior dynamic response characteristics.

From a task-space geometric perspective, the performance improvement achieved by EKF-based control becomes more intuitive. Figure 5(c) illustrates the comparison of end-effector trajectories in the *XY* plane. With EKF state estimation, the end-effector trajectory closely adheres to the ideal circular path, exhibiting a markedly higher geometric fidelity than the case using noisy measurement feedback alone. The overall smoothness and closure of the trajectory are significantly improved, indicating that the EKF plays a critical role in restoring task-space geometric consistency.

Table 2
Error statistics under noisy measurement feedback ($t = 0.3$–4.7 s).

Metric	End-effector position error $\|e\|$ (m)	*X*-axis position deviation (m)
Mean/*MAE*	0.0309	0.0118
RMSE	0.0325	0.0141
Maximum Error	0.067	0.0505

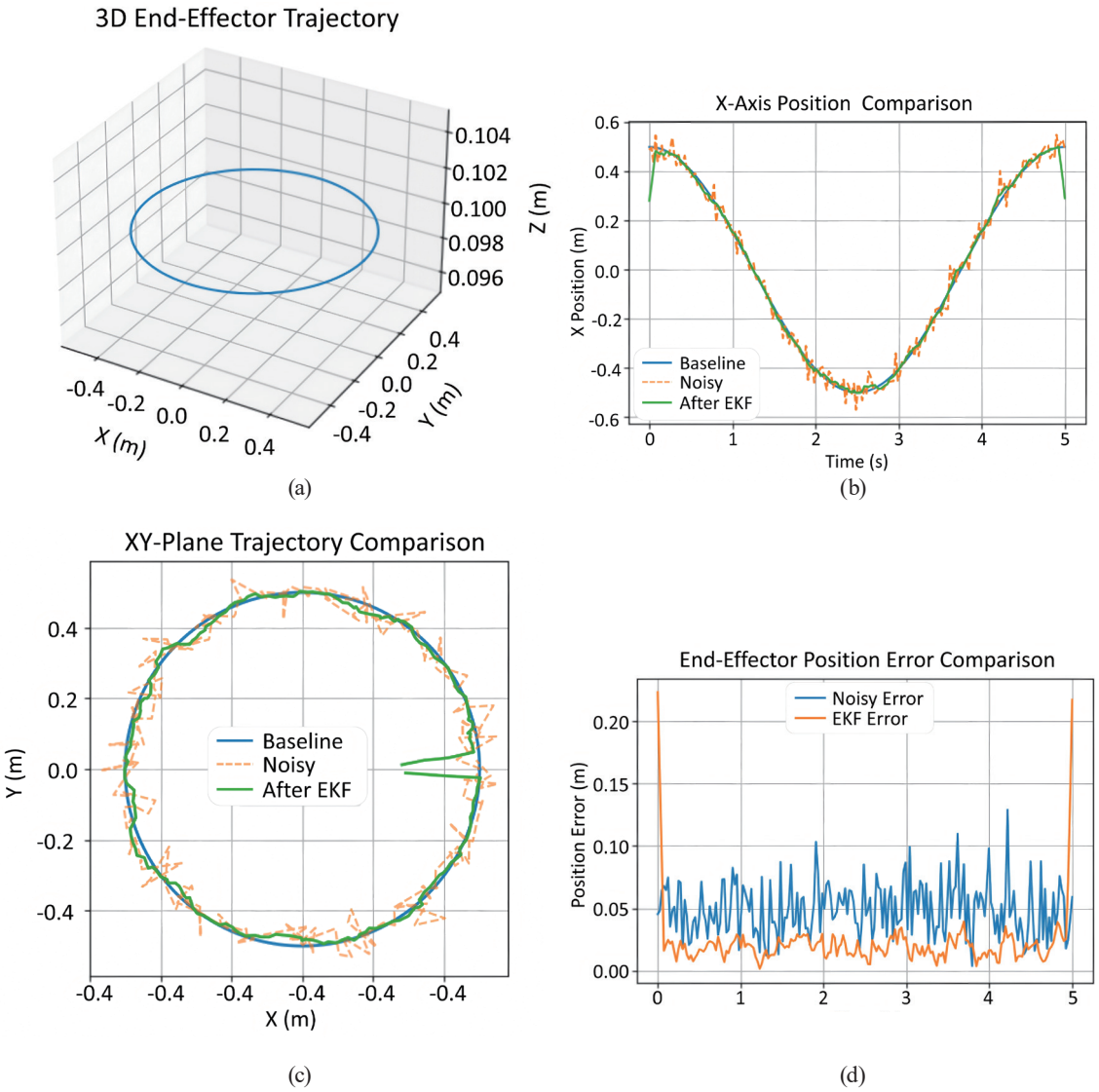

Fig. 5. (Color online) Performance improvement with EKF-based sensor fusion: (a) three-dimensional end-effector trajectory, (b) X-axis position comparison (baseline, noisy measurement, EKF), (c) XY trajectory comparison, and (d) position error comparison (with/without EKF).

To quantitatively evaluate the performance improvement, Fig. 5(d) shows a comparison of the time histories of end-effector position errors under noisy feedback control and EKF-based control. Over the entire simulation duration, the error magnitude under EKF-based control is consistently lower than that under direct noisy measurement feedback, with a more concentrated fluctuation range. These results demonstrate that EKF-based state estimation not only reduces instantaneous error levels but also effectively suppresses random error fluctuations, thereby significantly enhancing trajectory tracking accuracy and robustness.

With the introduction of EKF-based state estimation, the *X*-direction response exhibits a much closer adherence to the baseline trajectory, as shown in Fig. 5(b), with noisy oscillations being substantially suppressed. As shown in Table 3, statistical analysis over the steady-state

Table 3
Key performance metrics under two operating conditions (t = 0.3–4.7 s).

Metric	Noisy measurement feedback	EKF-based fusion control	Reduction (%)
Mean end-effector error	0.0563	0.0274	51.30
End-effector error *RMSE* (m)	0.0582	0.0281	51.60
Maximum end-effector error (m)	0.1103	0.0451	59.10
X-direction *MAE* (m)	0.0198	0.009	54.70
X-direction *RMSE* (m)	0.024	0.0108	54.90
Maximum *X*-direction deviation (m)	0.089	0.0312	64.90

interval indicates that, compared with the noisy measurement feedback case, the *MAE* of the *X*-direction deviation decreases from 0.0198 to 0.0090 m, the *RMSE* decreases from 0.0240 to 0.0108 m, and the maximum deviation decreases from 0.0890 to 0.0312 m. These results demonstrate the "noise reduction and stabilization" effect of the EKF on critical feedback variables.

From the perspective of end-effector position error, the EKF-based response maintains a consistently lower magnitude during the steady-state interval. As also shown in Table 3, the statistical results show that under EKF-based control, the mean end-effector position error is 0.0274 m, the *RMSE* is 0.0281 m, and the maximum error is 0.0451 m. Compared with noisy measurement feedback, the *RMSE* of the end-effector error is reduced by approximately 51.6% (from 0.0582 to 0.0281 m) and the maximum error is reduced by approximately 59.1% (from 0.1103 to 0.0451 m).

This simultaneous reduction in both error magnitude and fluctuation range indicates that the EKF not only lowers the average tracking error but also effectively suppresses error peaks that degrade trajectory quality.

6. Discussion

Under noisy conditions, trajectory fluctuations in robotic manipulator control often stem from measurement error propagation within the closed-loop structure, rather than inherent control law instability. Sensor noise directly affects position feedback, while velocity signals obtained via numerical differentiation suffer from amplified noise. This amplified noise is injected into the control input through derivative feedback and dynamic compensation terms, manifesting as oscillations in joint space and geometric deviations in task space.

The introduction of the EKF fundamentally alters the state estimation mechanism. State estimates are no longer solely reliant on instantaneous sensor readings but are constrained by model-based temporal prediction. Multisensor data are fused through statistical weighting, reducing the effects of individual noisy measurements. High-frequency disturbances are thus prevented from directly entering the control loop and are smoothed during the prediction-update process. This improves the temporal continuity of the system response, although the effectiveness remains dependent on model accuracy and the validity of noise assumptions.

Improved state estimation quality positively impacts the control layer. In computed torque control, nonlinear compensation terms are highly sensitive to velocity estimates. Noisy velocity

signals can cause fluctuations in these terms, even with small position errors. The EKF's model-based estimation enhances the temporal consistency of velocity signals, thereby stabilizing the compensation process. However, this does not fully eliminate noise effects. Factors such as modeling inaccuracies, non-Gaussian disturbances, actuator dynamics, and communication delays require further investigation in more realistic engineering environments. Furthermore, the results highlight the critical role of sensor bias stability and bandwidth in long-duration fusion accuracy, providing quantitative guidance for selecting MEMS IMUs and optical encoders. The proposed simulation framework can be used to evaluate how different sensor noise specifications affect final control performance, thereby supporting sensor design and system integration decisions.

7. Conclusion

In this paper, we proposed a closed-loop control strategy integrating multisensor fusion and an EKF to improve the trajectory tracking accuracy of a Puma 560 robotic manipulator under sensor noise. Kinematic, dynamic, and stochastic sensor models were established. An EKF was designed to fuse encoder and IMU data, providing accurate joint state estimates for a computed torque controller. Simulations demonstrate that this approach significantly reduces end-effector tracking error and suppresses noise propagation compared with conventional methods. Current work is limited to simulation; the results have not been validated on physical hardware, and factors such as sensor non-Gaussian noise, time delays, communication errors, and joint flexibility were not considered. Future efforts will focus on hardware-in-the-loop validation, adaptive robust filtering (e.g., adaptive EKF or particle filtering), and deep-earning-assisted noise modeling to address real-world industrial applications.

References

1 K. Lin, Q.-B. Ge, H. Li, and S. Chen: IEEE Trans. Autom. Sci. Eng. **22** (2025) 2318. https://doi.org/10.1109/TASE.2024.3378391
2 S. Yin, J. Zhang, L. Yu, and X.-S. Yang: Signal Process. **224** (2024) 109578. https://doi.org/10.1016/j.sigpro.2024.109578
3 D. Ostermeier, J. Külz, and M. Althoff: IEEE Rob. Autom. Lett. **10** (2025) 9964. https://doi.org/10.1109/LRA.2025.3597897
4 E. Mounier, M. Karaim, M. Korenberg, and A. Noureldin: IEEE Sens. J. **25** (2025) 9998. https://doi.org/10.1109/JSEN.2025.3536806
5 Q.-B. Ge, Z.-H. Song, B.-T. Zhu, and B.-J. Zhang: Chin. J. Aeronaut. **37** (2024) 232. https://doi.org/10.1016/j.cja.2024.04.016
6 B.-H. Li, J. Li, J.-H. Gu, and S.-Q. Li: Europhys. Lett. **152** (2025) 42001. https://doi.org/10.1209/0295-5075/ae0fc1
7 Z.-H. Jiang, W.-G. Zhou, H. Li, Y. Mo, W.-C. Ni, and Q. Huang: IEEE Trans. Ind. Electron. **65** (2018) 3337. https://doi.org/10.1109/TIE.2017.2748058
8 Y. Chen, J.-W. Ding, Y. Chen, and D. Yang: Appl. Sci.-Basel **14** (2024) 2219. https://doi.org/10.3390/app14052219
9 G.-T. Tian and G.-R. Duan: Int. J. Robust Nonlinear Control **33** (2023) 1750. https://doi.org/10.1002/rnc.6450
10 R. Yildiz, M. Barut, and E. Zerdali: IEEE Trans. Ind. Inf. **16** (2020) 6423. https://doi.org/10.1109/TII.2020.2964876
11 J.-Q. Si, Y.-X. Niu, and B.-T. Wang: Sensors **25** (2025) 6462. https://doi.org/10.3390/s25206462

12 J.-N. Fu, X.-Y. Liu, Y.-Q. Liu, Z. Chen, and B. Yao: ISA Trans. **149** (2024) 373. https://doi.org/10.1016/j.isatra.2024.04.012
13 P.-L. Wu, Y.-C. Hung, and J.-S. Shaw: Proc. Inst. Mech. Eng., Part C: J. Mech. Eng. Sci. **236** (2022) 9753. https://doi.org/10.1177/09544062221096946
14 Y. Li, P.-W. Zhang, J.-Y. Yu, K.-Y. Zou, X.-G. Jia, J.-W. Yang, and J. Bao: Sens. Mater. **37** (2025) 3119. https://doi.org/10.18494/SAM5629
15 T. Kruse, T. Griebel, and K. Graichen: IEEE Access **13** (2025) 11863. https://doi.org/10.1109/ACCESS.2025.3528348
16 J. McElreath, D. E. J. van Wijk, and M. Majji: IEEE Trans. Aerosp. Electron. Syst. **61** (2025) 9460. https://doi.org/10.1109/TAES.2025.3552071
17 X. Liu, Z.-G. Ren, H.-Q. Lyu, Z.-H. Jiang, P.-J. Ren, and B.-D. Chen: IEEE Trans. Syst. Man Cybern.: Syst. **51** (2021) 3093. https://doi.org/10.1109/TSMC.2019.2917712